



A Point Process Analysis of Sensory Encoding

GARRETT B. STANLEY

Division of Engineering & Applied Sciences, Harvard University, Cambridge, MA 02138, USA

gstanley@deas.harvard.edu

ROXANNA M. WEBBER

Harvard-MIT Division of Health Sciences & Technology, Cambridge, MA 02138, USA

webber@fas.harvard.edu

Received January 7, 2003; Revised June 25, 2003; Accepted July 7, 2003

Action Editor: Barry J. Richmond

Abstract. Nowhere is the sparse nature of neuronal coding more evident than in the sensory cortex, where neuronal response becomes increasingly tuned to specific features of the sensory environment. For such situations, where rate modulation schemes do not accurately describe the neuronal response to sensory stimuli, statistical descriptions based on point process events are particularly appropriate. Here, intensity measures derived from experimental data in the rat somatosensory cortex enable the direct analysis of statistical structure within spike trains, as well as inter-relationships between tactile stimuli and neuronal response. Intensity measures capture structure in spontaneous as well as driven activity, reflecting the interplay between excitatory and suppressive influences on neuronal firing. Second-order intensity estimates reveal strong dependencies upon patterns of tactile stimulation, which define the neuronal response characteristics to temporally structured stimuli.

Keywords: barrel cortex, vibrissa, stochastic

1. Introduction

Rats and other rodents have arrays of facial whiskers (vibrissae) that are vital for survival; neonates deprived of their vibrissa exhibit severely impaired behavioral development (Carvell and Simons, 1996). By actively palpating objects, rats have also been shown to be able to discriminate between very similarly textured surfaces based on vibrissa exploration alone (Guic-Robles et al., 1989; Carvell and Simons, 1990), illustrating the exquisite sensitivity of this sensory modality. Unlike the vigorous responses observed in the trigeminal (Lichtenstein et al., 1990) and thalamic nuclei (Simons and Carvell, 1989; Nicolelis and Chapin, 1994), the individual cortical cells corresponding to the facial vibrissa are quite sparse in their response to mechanical

deflections of the vibrissa (Simons, 1978). For this reason, firing rate measures often used in early sensory pathways are not ideal for describing the cortical activity. Here, we present point process measures with well-defined statistical properties for characterizing spontaneous activity and activity induced through controlled vibrissa deflection. Specifically, intensity measures are developed to characterize the correlation structure in spontaneous spiking, as well as corresponding cross-intensity measures for describing the causal relationships between vibrissa deflection and neuronal spiking. Importantly, the correlation structure reflects the interplay between transient excitatory and long-lasting suppressive influences that defines neuronal response characteristics to temporally structured stimuli. The second-order effects are shown to dramatically

influence the neuronal activity in response to stimulus patterns over time. Finally, an approach to capturing the non-stationary properties in stimulus/response relationships is presented for rapid adaptation to periodic mechanical stimuli. The approach developed here provides a general framework for capturing the subtle dynamics in sensory cortices where temporally sparse activity is a ubiquitous characteristic of neuronal encoding.

2. Methods

2.1. Animal Preparation

Adult female albino rats (Sprague-Dawley; 250–300 g) were used for all experiments. An initial dose of sodium pentobarbital (50 mg/kg, IP) was administered and supplemental pentobarbital IP was given as needed to maintain a surgical plane of anesthesia (Zhu and Connors, 1999; Ghazanfar et al., 2000). Depth of anesthesia was monitored through continuous measures of heart rate and respiration, and through eyelid/pedal reflexes and response to aversive stimuli (toe or tail pinch). Otic drops were placed in the ears, and the animal was then mounted on a stereotaxic device with a thermostatically controlled heating pad set to 38°C. Topical lidocaine was applied to all areas of incisions, and the surgical area was prepared with a betadine solution. Atropine (0.05 mg/kg, IP) was then given to minimize buildup of fluid in airways, and Ringers solution (1–2 ml, SC) given periodically to prevent dehydration. Following a midline incision, skin and tissue were resected, and connective tissue removed. A small craniotomy (~2 mm in diameter) was performed directly above the barrel field, but leaving the dura mater intact. Bone wax was used to create a dam, and the cortex was then covered with a mineral oil solution to help stabilize the recording. Supplemental doses of sodium pentobarbital were given as necessary to maintain a light level of anesthesia during recording (typically 12 mg/kg/hr). At the end of the recording session, the animal was euthanized with an overdose of sodium pentobarbital. All procedures were approved by the Animal Care and Use Committee at Harvard University.

2.2. Physiological Recording

Single tungsten microelectrodes (5–10 M Ω , FHC Inc., Bowdoinham, ME) were used to obtain single unit ex-

tracellular recordings. Microelectrodes were advanced into the tissue to depths commensurate with cortical layer 4 (500–900 μ m, (Simons, 1978; Moore and Nelson, 1998)). Receptive fields were mapped using manual techniques to determine receptive field (RF) extent and primary whisker (PW) location. For each recorded neuron, the whisker location of the primary whisker (i.e. D1, C3, etc.) is indicated in the figure legends, according to the established nomenclature of the rows and arcs of the whiskers on the facial pad (Welker, 1971). The action potential waveform of fast spiking units (FSUs) is approximately half the duration of regular spiking unit (RSU) waveforms (Simons, 1978; Zhu and Connors, 1999). We therefore utilize waveform duration, along with the relative RF size, for discriminating the cell types. By selecting cells with narrowly focused RFs (typically single vibrissa) and action potential waveforms of longer duration (total duration \approx 1.5 ms), we have limited the current study to that of RSUs. The data collection and actuator were controlled using routines written in C++ within the LabWindows acquisition/control software environment (National Instruments, Austin, TX). Neuronal signals were first amplified (A-M Systems, Sequim, WA), and then acquired using a National Instruments signal conditioning unit fed to an A/D board (sampling at 20 kHz/channel) in the data acquisition computer. Single unit activity was discriminated using standard template matching techniques and physiologically plausible refractory periods (Lewicki, 1998). Specifically, waveforms were first obtained using a simple threshold. Several parameters were then used to discriminate single units, including amplitudes of the peak and trough of the waveforms, time to peak, and time to trough. For each neuron recorded from experimentally, the receptive field was qualitatively assessed and spontaneous data were collected.

2.3. Vibrissa Stimulation and Data Acquisition

The whisker deflection was controlled with a multi-layered piezoelectric bending actuator with a range of motion of 1 mm over a bandwidth of 200 Hz (Polytech PI, Auburn, MA). The actuator deflection was calibrated using a photo-diode circuit and an XYZ positioner to determine the relationship between input voltages and steady state deflection. The actuator was positioned at a location 10 mm from the face and the whisker was inserted into a 4 cm section of 20 μ L glass pipette glued to the end of the actuator (approximately

0.57° per 100 μm deflection). An effective stimulus for driving the cells is a square wave in deflection, whose dynamics can be represented as:

$$s_\gamma(t) = \begin{cases} 1 & \text{for } k \leq t < k + \gamma \\ 0 & \text{for } k + \gamma \leq t < k + 1 \end{cases} \quad (1)$$

for $k = 0, 1, \dots$, where $100 \times \gamma$ is the duty cycle, which represents the percentage of time the wave is nonzero. For a square wave of frequency f_s (in Hz) and amplitude \bar{d} , the deflection pattern is then described as $d(t) = \bar{d}s_\gamma(f_s t)$, where \bar{d} is the maximum deflection (700 μm). Pure square waves in deflection produce mechanical ringing of the piezoelectric actuator, which can in some cases induce artifactual responses in neuronal recordings (Simons, 1983). The square waves were thus filtered with a causal Gaussian function $g(t)$ to minimize ringing:

$$d_s(t) = \int_0^t g(\tau)d(t - \tau) d\tau \quad (2)$$

$$g(t) = 2 \times \frac{1}{\sqrt{2\pi\sigma_g^2}} \exp\left\{-\frac{t^2}{2\sigma_g^2}\right\}$$

where $d_s(t)$ is the smoothed deflection pattern and σ_g is the standard deviation of the Gaussian filter. Again, using a photodiode calibration circuit, we found a range of σ_g that limits velocities to 100–155 mm/sec and limits the amplitude of ringing to acceptable levels (causing no detectable neuronal response). Vibrissa were deflected in the rostral-caudal plane.

For aperiodic stimuli (i.e. random intervals), the stimulus can be expressed as $d(t) = \bar{d}s_{\sigma,\alpha}(t)$, where:

$$s_{\sigma,\alpha}(t) = \begin{cases} 1 & \text{for } \sigma_k \leq t < \alpha_k \\ 0 & \text{for } \alpha_k \leq t < \sigma_{k+1} \end{cases} \quad (3)$$

for $k = 0, 1, \dots$, and the σ_k and α_k represent the times of the k th rising and falling edges, respectively. The intervals $\alpha_k - \sigma_k$ and $\sigma_{k+1} - \alpha_k$ were independent draws from a uniform distribution on 15 to 250 ms. As before, the square waves were convolved with a Gaussian window to eliminate ringing. Random stimulus trials were repeated multiple times.

2.4. Statistical Analyses

Suppose that for all discussions, the spike train is represented as a stochastic point process Y on the interval

$(0, T]$, with counting measure $N_Y(t)$ representing the number of events in the interval $(0, t]$. Let the event times of a process Y over the interval $(0, T]$ be denoted as $\tau_0 \leq \tau_1 \leq \dots \leq \tau_k$, with corresponding inter-spike intervals (ISIs) $\tau_k - \tau_{k-1}$. Let the mean interval be denoted μ . If the process is a homogeneous Poisson process, the observed intervals will be exponentially distributed with parameter $\lambda = 1/\mu$.

2.4.1. Auto-Intensity Estimates. The temporal correlation structure of the observed processes is often revealing of the underlying neuronal mechanisms. The auto-intensity function is such a measure, and is defined as (Perkel et al., 1967a; Brillinger et al., 1976; Cox and Isham, 1980):

$$m_{YY}(u) = \lim_{h \rightarrow 0} \frac{Pr\{Y \text{ spike in } (t, t + h] \mid Y \text{ spike at } t - u\}}{h} \quad (4)$$

as depicted in a of Fig. 1. The auto-intensity function is defined in the limit as h goes to zero, whereas, in practice, averaging must be performed over finite bin-widths. This quantity is estimated in practice as:

$$\hat{m}_{YY}(u) = \frac{\#\{u - \frac{h}{2} < \tau_k - \tau_j < u + \frac{h}{2} : \forall k, j\}}{hN_Y(T)}$$

where $\#$ represents the number of τ_k that satisfy this constraint for a particular τ_j , and h is the bin-width, taken to be sufficiently small. The term $N_Y(T)$ is the spike count over the entire interval $(0, T]$. Note that for a finite bin-width and small values of the lag u , the occurrence of a spike at time $t - u$ guarantees the occurrence of a spike in the window $(t, t + h]$ (i.e. the process is perfectly correlated for zero lag). The square-root intensity is presented due to the simplified form of the estimator variance (Brillinger et al., 1976). An independent process would have a mean of $\sqrt{m_Y}$ and a 95% confidence interval of $\pm 1/\sqrt{hN_Y(T)}$ around $\sqrt{m_Y}$, where m_Y is the mean rate of the process Y .

2.4.2. Measure of Bursting. Neurons often generate bursts of action potentials in quick succession, which along with refractoriness, represents a clear deviation from a homogeneous Poisson process. As a measure of the bursting, the fraction of spikes in the train that are involved in a burst can be computed. Here, a burst is defined as any sequence of action potentials having inter-spike intervals (ISIs) less than 20 ms. So,

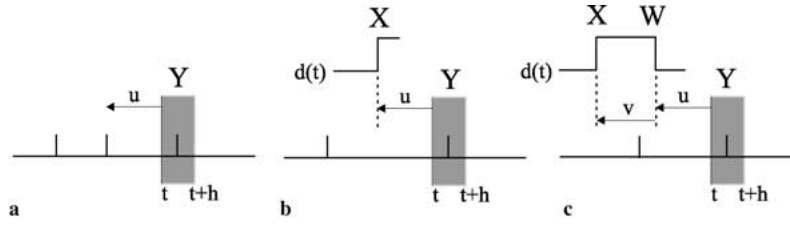


Figure 1. Intensity estimation. (a) Auto-intensity function $m_{YY}(u)$ characterizes relationship between pairs of events in train. (b) Cross-intensity estimate $m_{XY}(u)$ between the rising edge of the stimulus and the neuronal response. (c) Second-order cross-intensity estimate $m_{XWY}(u, v)$ describes the influence of rising and falling edge interactions on neuronal response.

for example, a burst of two action potentials would contribute 2 to the cumulative sum, while a burst of three action potentials would contribute 3 to the cumulative sum, and so on. The fraction is then computed as the number of spikes involved in a burst divided by the total number of spikes in a trial. Note that this measure does, by construction, increase as the mean rate increases.

2.4.3. Cross-Intensity Estimates. The barrel neurons are primarily sensitive to vibrissa velocity rather than amplitude (Ito, 1981; Pinto et al., 2000). In our stimulus paradigm, the primary vibrissa undergoes approximate step changes in deflection, effectively resulting in impulses in vibrissa velocity. Suppose that the rising edge of the deflection square wave can be described as a point process X with event times $\sigma_0, \sigma_1, \dots$. We can then describe the cross-intensity between the stimulus events (rising edges) and the corresponding evoked neuronal events:

$$m_{XY}(u) = \lim_{h \rightarrow 0} \frac{\Pr\{Y \text{ spike in } (t, t+h] | X \text{ event at } t-u\}}{h} \quad (5)$$

which can be estimated as:

$$\hat{m}_{XY}(u) = \frac{\#\{u - \frac{h}{2} < \tau_k - \sigma_j < u + \frac{h}{2} : \forall k, j\}}{hN_Y(T)} \quad (6)$$

As with the auto-intensity, an independent square-root cross-intensity would have mean $\sqrt{m_Y}$ and 95% confidence intervals of $\pm 1/\sqrt{h}N_X(T)$ around $\sqrt{m_Y}$. If the falling edge deflections can be described as a point process W , an analogous cross-intensity, $m_{WY}(u)$ can be determined using identical measures as described

in Eqs. (5) and (6). The procedure is depicted in b of Fig. 1.

2.4.4. Higher-Order Interactions. The intensity measures introduced above only account for first-order interactions. In many cases, higher-order interactions exist between events over time, or between multiple processes. Because the vibrissa is undergoing deflections from 0 to the maximum deflection and back, in a sequence of deflections the rising edge (deflection in the positive direction) is always preceded by a falling edge (deflection in the negative direction). For relatively small differences in deflection times, the neuron is under the influence of not just the most recent stimulus event, but also the event preceding. A second order cross-intensity measure can be formed (Brillinger et al., 1976) that takes into consideration the temporal relationship between the rising and falling edges of the deflection patterns:

$$m_{XWY}(u, v) = \lim_{h \rightarrow 0} \frac{\Pr\{Y \text{ spike in } (t, t+h] | W \text{ event at } t-u, X \text{ event at } t-(u+v)\}}{h}$$

where W is the process of events related to the falling edge, and X is the process of events related to the rising edge. Estimates are generated in much the same manner as described with the first-order cross-intensity function in Eq. (6). The procedure is depicted in c of Fig. 1.

2.4.5. Adaptive Estimation. The statistical estimators described thus far assume that the relationships are dynamic, but time-invariant (i.e. that the stimulus/response relationship does not change with time). However, the neurons typically display an adaptation to periodic stimuli which violates this assumption (Ahissar et al., 2001; Chung et al., 2002). The estimate in Eq. (5), therefore, would represent a steady state relationship, but would not reflect the nature of the

adaptation. We therefore designed stimuli to directly probe this issue. Suppose that a square wave stimulus of frequency f_s is turned on and off at a frequency f_a (adaptation frequency). We can represent the resulting stimulus mathematically as the product of two square waves:

$$d(t) = \bar{d}s_{\gamma_s}(f_s t)s_{\gamma_a}(f_a t)$$

where γ_s and γ_a represent the duty cycles for the deflection pattern and the adapting stimulus, respectively ($\gamma_s = \gamma_a = 0.5$). As before, the stimulus $d(t)$ is convolved with a smoothing filter to produce the smoothed stimulus $d_s(t)$. Using such a probe, the adaptation effects can be directly assessed. Effectively, the cross-intensity measures previously described no longer assume that the relationship only depends on the relative time difference between stimulus event and response, u , but instead depends on the absolute times of the stimulus events and responses within the period of the adapting stimulus:

$$m_{XY}(t_1, t_2) = \lim_{h \rightarrow 0} \frac{\Pr\{Y \text{ spike in } (t_2, t_2 + h) \mid X \text{ event at } t_1\}}{h} \quad (7)$$

for $t_1 \leq t_2 < t_1 + 1/2f_s$, and $t_1 = t - k/f_a$ for $k = 0, 1, \dots$. Note that this can also be expressed as $m_{XY}(t_1, u)$, where $u = t_2 - t_1$, and represents a lag relative to the absolute time t_1 .

2.4.6. Simulation. Once the intensity measures have been estimated from data, the response of the system can be simulated. For example, consider the auto-intensity measure introduced in (4). Given a spike at time t , the quantity $h\hat{m}_{YY}(u)$ represents the probability that a spike occurs in the interval $(t + u - h/2, t + u + h/2]$, for small h , which is equivalent to an inhomogeneous Poisson process. In practice, therefore, conditioned on a spike at time t , an inhomogeneous Poisson process is simulated, and only the first spike is retained. This spike is then conditioned upon to produce the subsequent spike, and so on. To simulate stimulus-driven processes, a similar approach is used, except that the conditioning occurs on the stimulus events. An inhomogeneous Poisson can be simulated using the binomial distribution as an approximation of the Poisson distribution. At each time step, a draw is made from a uniform distribution on $[0, 1]$. If the quantity $h\hat{m}_{YY}$ is greater than the random draw, a spike is generated.

Note that this approximation of the Poisson distribution with the binomial is valid only when $h\hat{m}_{YY}$ is small (less than 2% deviation in the density for $n = 1$ and $p = h\hat{m}_{YY} < 0.2$), which is the case for the simulations presented here.

3. Results

3.1. Spontaneous Activity

In general, barrel neurons do not have high spontaneous firing rates. Brumberg et al. reported that putative regular-spiking, excitatory units exhibit spontaneous rates below 2 Hz (Brumberg et al., 1996). Nonetheless, the statistical properties of the spontaneous activity can reveal much about the underlying functional properties of the cell. Given spike times τ_0, τ_1, \dots , the interspike-interval (ISI) is defined as $\tau_k - \tau_{k-1}$. The histograms of the ISIs for three characteristic neurons are shown in Fig. 2a–c, with the theoretical result for a homogeneous Poisson process at the same mean rate presented with the solid curve (as described in the methods). For the neuron shown in a, the distribution of ISIs exhibits a large peak just after the refractory period. There was a larger number of intervals at around 10 ms than would be predicted by the exponential distribution. This is due to the burstiness of the cell, where a sequence of action potentials with very short ISIs occur in rapid succession. However, the remainder of the distribution appears nearly exponential. The time resolution of the histogram plot does not clearly reveal deviations related to the refractory period, but upon closer inspection, the cells do not tend to exhibit ISIs below approximately 10 ms. In addition to the burst-related peak in the ISI histogram in a, the neurons in b and c exhibit other strong deviations from Poisson-like behavior. The neuron in b exhibits a deviation from the exponential distribution in that the number of observed ISIs for the range from approximately 50 to 150 ms is significantly below that which would be expected from a homogeneous Poisson process. Note that the approximate depth of recording for the cell shown in b is 1300 μm , which would suggest layer 5, although without the histological characterization, it cannot be stated with certainty. The neuron in c exhibits a deviation from the exponential distribution through a lack of representative ISIs in the 50 to 150 ms range as in b, but also through an oscillation that results in an interval distribution that is at times below and at times above that expected for a homogeneous Poisson process.

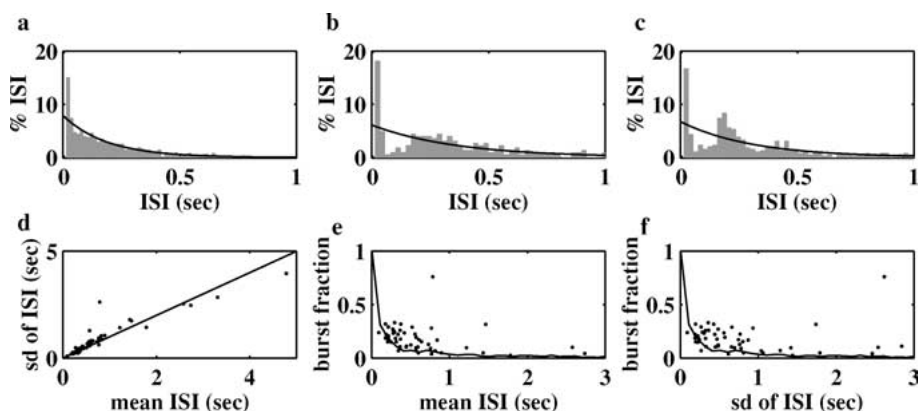


Figure 2. Statistics of interspike intervals. (a–c) Each panel is the histogram of interspike intervals for a different neuron, obtained from spontaneous activity of the cell over a 2 minute trial, with the theoretical curve for a homogeneous Poisson process of the same mean rate superimposed (for each cell, depth of recording site, primary whisker, and mean spontaneous rate—a: 600 μm , D1, 5.3 Hz; b: 1300 μm , C2, 1.3 Hz; c: 800 μm , D2, 3.2 Hz). (d–f) Mean ISI versus the standard deviation (SD) of the ISIs for 52 cells from 20 rats, fraction of spikes involved in a burst versus the mean ISI for each of the cells, and the same versus the SD of ISIs for each of the cells, respectively. Superimposed on e and f are curves representing the mean burst fraction observed for repeated simulations of a homogeneous Poisson process at each mean rate.

Spontaneous data were collected from 52 cells in 20 rats, and the summary statistics are presented in the bottom row of Fig. 2. We found that the characteristics shown in Fig. 2a, b, and c were present in approximately 10, 60, and 30% of the cells within the population, respectively. The standard deviation (SD) of the ISIs is plotted against the mean of the ISIs for each cell in the population in d. The line represents the condition where the SD is equal to the mean (i.e. coefficient of variation = 1), which is what would be expected for the exponential distribution. The only apparent trend is that at high firing rates (low mean ISI), the cells tend to be supra-Poisson in terms of the variability, and at lower firing rates, the cells tend to be sub-Poisson in their variability. The burst fraction (fraction of spikes involved in a burst, see methods) is plotted against the mean ISI and the SD of the ISIs for each cell in e and f, respectively. The solid curve for both represents the burst fraction that would be expected from a homogeneous Poisson, obtained through repeated simulations of a homogeneous Poisson at different mean rates. Note that the measure of burstiness that we have defined naturally increases with an increasing rate. However, even taking this effect into account, the spontaneous activity of the barrel neurons tends to exhibit more bursts than would be expected from a homogeneous Poisson.

The ISI histograms only show the distribution of intervals, disregarding the temporal correlation structure of the spike train. In order to more carefully explore the nature of the temporal correlation structure of the neu-

ronal activity, the auto-intensity function $m_{YY}(u)$ was estimated for the spontaneous activity of each of the cells shown in Fig. 2, and the results are shown in Fig. 3. The top panels of a–c represent the raster of spikes surrounding each spike of the trial for each cell, and the bottom panels represent the corresponding square-root auto-intensity function, as defined in the methods. It should be noted that these raster plots are different from traditional raster plots in that each row does not represent a separate trial, but instead represents a collection of the spikes that occur relative to a different individual spike *within* the same trial. The gray bar represents a 95% confidence interval around the mean level on an uncorrelated process. The first cell, shown in a, exhibits an intensity that is statistically different from the mean only at zero lag. This correlation structure is shared by the homogeneous Poisson process, which also exhibits an auto-intensity that is equal to the mean rate for non-zero lags and has a sharp positive peak at zero-lag. The second cell, shown in b, exhibits suppressive lobes for lags between 50 and 150 ms that extend out of the confidence band. The third cell, shown in c, exhibits a suppressive lobe for lags between 50 and 150 ms, an excitatory lobe between 170 and 200 ms, and an additional suppressive lobe from 270 to 310 ms. The difference in structure between b and c could be a result of the variability of the response. Oscillatory behavior could indeed exist in b, but a weak oscillation results in temporal variability in the spiking activity, which causes it to be averaged out in the intensity estimate.

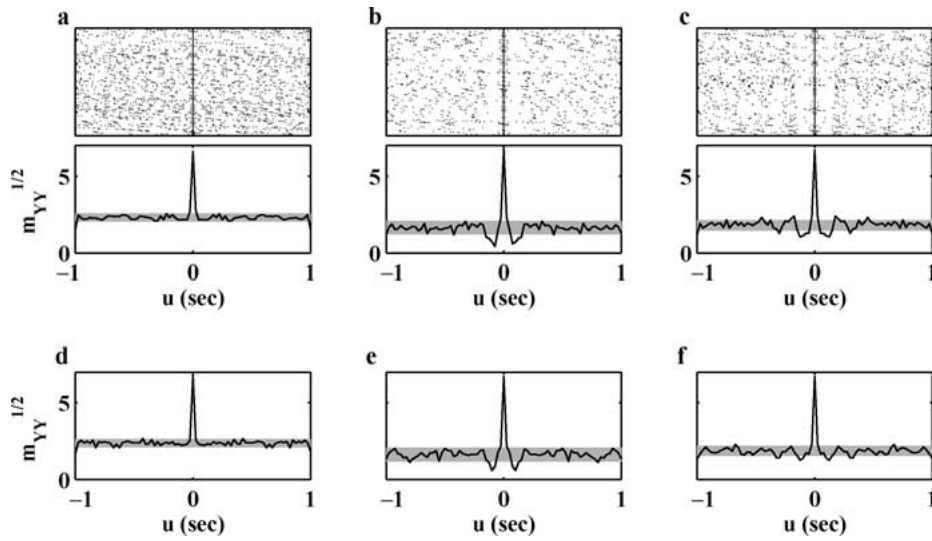


Figure 3. Correlation structure of spontaneous activity. (a–c) For cells shown in Fig. 2, raster of spikes surrounding each spike of the trial (top), and the square-root auto-intensity function (bottom) for the spontaneous activity, with the null-band of an uncorrelated process shown with the gray band ($h = 25$ ms). The horizontal axis represents time relative to individual spike. (d–f) Auto-intensity estimates ($h = 25$ ms) from simulated spontaneous activity based on auto-intensity estimates from recorded responses in a–c. The horizontal axis represents time relative to individual spike.

Note also that the bin-width was set to $h = 25$ ms to most clearly demonstrate the suppression in panels b and c, but a bin-width of this size smooths out the effects of the short burst intervals seen in Fig. 2. Panels d–f show the corresponding auto-intensity estimates for simulations of the spontaneous processes, based solely on the first order measures shown in the bottom row of a–c. As discussed in the methods, the intensity values obtained here, along with the bin-size, produced probabilities that were small enough as to allow the use of a binomial approximation for the simulations. The auto-intensity estimates for the simulated processes, which are nearly identical to the auto-intensity measures of the recorded processes, serve as a simple method of evaluating self-consistency in the simulations. Higher-order auto-intensity measures revealed no apparent structure beyond that revealed through m_{YY} (data not shown).

3.2. Step Response

When the primary whisker is stimulated with a step-change in deflection, the barrel neurons typically respond with a transient excitatory response after a short latency of 5–15 ms. For a typical barrel neuron, the ISI histogram and corresponding auto-intensity function in response to a square wave deflection pattern are shown in a and b of Fig. 4. The stimulus in this case

was a 1 Hz square wave with a 20% duty cycle ($f_s = 1$ Hz, $\gamma = 0.2$) with smoothed edges, as described in the experimental methods. The histogram for the number of spikes in the 200 ms following the rising edge of the stimulus is shown in c. It is clear that even when driven, this cell usually fires only one spike, and more rarely zero or two spikes (mean approx 1.3 spikes for each deflection presentation, indicated by arrow). The histogram for the response latency, which is defined as the time to the first spike for the cases in which a spike occurs in the 20 ms following the stimulus (mean 6.8 ms, indicated by arrow), is shown for this cell in d. The correlation structure of the stimulus/response relationship is revealed through the cross-intensity functions relating the neuronal process Y to the rising and falling edges of the stimulus. For the process defined by the rising edge, X , the corresponding raster and estimate of $\sqrt{m_{XY}(u)}$ are shown in panels e and f, respectively of Fig. 4. This particular cell was shown to have similar response to the falling edge of the stimulus (not shown), but some cells exhibit distinct asymmetries due to strong directional tuning (Simons, 1978). Also note that the activity is not sustained during the plateau of the deflection, consistent with the phasic response seen in a majority of neurons in the barrel cortex (Simons, 1978). Using the simulation techniques described in the methods section, the response of the cell to the square wave

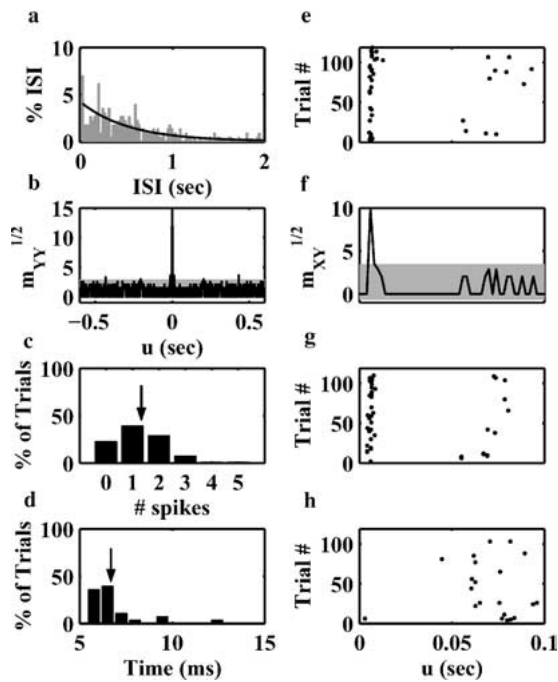


Figure 4. Response to square wave deflection. (a) ISI histogram in response to a square wave at 1 Hz with a 20% duty cycle. (b) The square-root auto-intensity function for the trial, where the gray band represents a 95% confidence interval on an uncorrelated process, and the horizontal axis is time relative to an individual spike. (c, d) Average number of spikes following a rising edge of the deflection (arrow indicates mean, 1.3 spikes), and the time to the first spike following a rising edge in deflection (arrow indicates mean, 6.8 ms), respectively. (e, f) Raster and corresponding square-root cross-intensity for the rising edge response to repeated deflections of the primary whisker. (g) Raster response simulated from cross-intensity function in f. (h) Raster for response to square wave at 1 Hz with 96% duty cycle ($h = 2$ ms, depth = 500 μ m, PW D4). For e–h, horizontal axis, u , is time since rising edge in deflection.

was simulated using the cross-intensity functions m_{XY} and m_{WY} to drive an inhomogeneous Poisson process, conditioned on the stimulus events. For the rising edge response, the raster plot of the simulated spiking activity is shown in g. As a validation, the cross-intensity between the rising edge events and the neuronal response was estimated from the simulated process, resulting in a measure that is indistinguishable from that involving the recorded process (not shown). However, when the periodic structure of the stimulus is varied, the cross-intensity function does not predict the higher order interactions observed. The raster plot for the response of the cell to a 1 Hz square wave with 96% duty cycle (i.e. deflected for 960 ms, at rest position for 40 ms) in which the rising edge is preceded 40 ms earlier by a

falling edge of the stimulus is shown in h. The lack of responsiveness suggests higher-order interactions that are not accounted for by the cross-intensity function m_{XY} . To explore this phenomenon more carefully, the timing between rising and falling edges of the square wave was varied for a different cell, shown in Fig. 5.

For a square wave at 1 Hz ($f_s = 1$ Hz), varying the duty cycle results in varying degrees of interactions between rising and falling edges of the stimulus. A duty cycle of γ results in a $(\gamma \times 1000)$ ms interval between a rising edge and the subsequent falling edge, and a $((1 - \gamma) \times 1000)$ ms interval between a falling edge and the subsequent rising edge. The stimuli for $\gamma = 0.1, 0.08, 0.05$ and 0.03 are superimposed on the cell's square-root auto-intensity function in the top row of a–d. The corresponding square roots of the estimates of the falling edge cross-intensity function m_{WY} are shown in the bottom row of a–d, along with the corresponding 95% confidence bands. The cross-intensity conditioned on the falling edge is greatly affected by the relative time of the preceding rising edge. In a and b, the long interval to the preceding rising edge (100 and 80 ms, respectively) results in a fairly strong intensity measure conditioned on the falling edge. The reduction of this interval to 50 ms in c results in an appreciable attenuation of the cross-intensity function. Finally, when the interval is reduced to 30 ms in d, the cross-intensity function is completely suppressed. A summary of this effect for different duty cycles is shown in the contour plot of the square-root second-order cross-intensity function $\sqrt{m_{XWY}}$ in e, where the response is completely suppressed for small values of the inter-deflection interval (v), but gradually grows as the preceding stimulus edge is further in the past. The arrow indicates time relative to stimulus edge for which the response was maximal.

The estimates of the second order cross-intensities shown in e of Fig. 5 resulted from separate trials of varying duty cycle. One interesting issue has to do with the response of the neuron to deflection patterns of random inter-deflection intervals, as would be experienced as the animal's own whisking activity drags the vibrissa across a textured surface. Such a trial is shown in Fig. 6 for the same cell. The stimulus in this case was a random binary pattern of deflection, with intervals ranging from 15 to 250 ms, as described in the methods section. The ISI histogram and auto-intensity estimate are shown in a and b, respectively. Visual inspection of the raster plot to repeated trials of the binary stimulus (c) reveals a clear driving of the cell by some of the edges

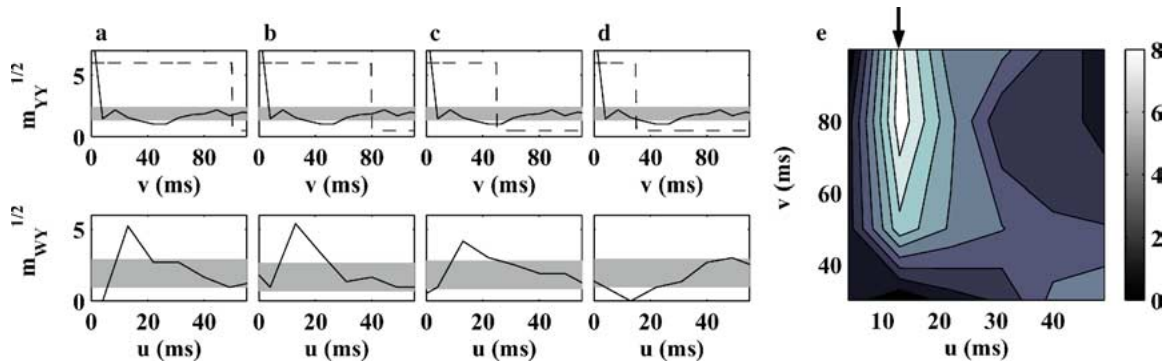


Figure 5. Effect of inter-deflection interval. (a–d) 1 Hz Square wave stimulus for duty cycles of 10, 8, 5, and 3% superimposed on spontaneous auto-intensity ($h = 9$ ms; horizontal axis is time relative to individual spike) shown in the top row. Bottom row shows corresponding cross-intensity estimates ($h = 9$ ms) for the falling edge response, where horizontal axis is time since falling edge deflection. (e) Square-root second-order cross-intensity estimate $\sqrt{m_{XY}(u, v)}$. Horizontal axis, u , is time since falling edge deflection, and the vertical axis, v , represents time between rising edge and falling edge deflection (see methods). Arrow indicates value of u with peak response (12 ms). For all panels, depth = 700 μm and primary whisker E4.

of the deflection pattern (shown, for example, by the vertical pattern of activity in the raster at approximately 2.1 seconds), while exhibiting little or no consistent activity in response to other edges. This is primarily due to

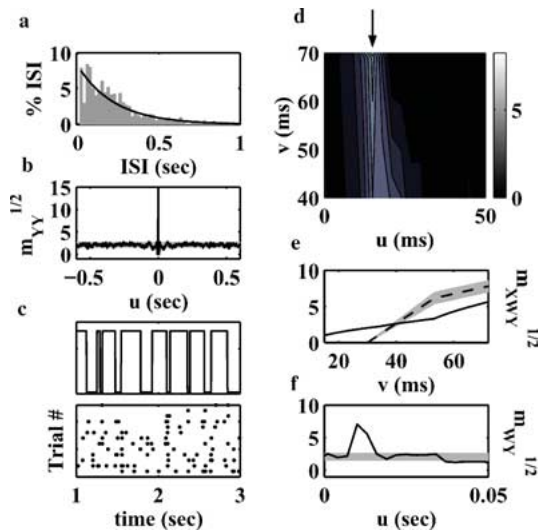


Figure 6. Response to random stimulus pattern. (a, b) ISI histogram and auto-intensity function estimate for the response to the binary pattern ($h = 3$ ms; horizontal axis is time relative to individual spike). (c) Random binary deflection pattern over 2 seconds, and the corresponding raster plot for 13 trials. (d) Square-root second-order cross-intensity estimate as a function of inter-deflection interval, v , and the time since the falling edge u ($h = 3$ ms, depth = 700 μm , E2, mean rate 2.9 Hz, arrow indicates value of u with peak response). (e) Peak square-root cross-intensity for randomized (solid) and separate (dashed, with gray band indicating standard error) trials as a function of v , at a fixed delay of $u = 12$ ms. (f) Square-root cross-intensity function estimate from binary stimulus ($h = 3$ ms). For all panels, depth = 700 μm and primary whisker E4.

the dependence of the neuronal activity on the temporal history of timings between deflections within the patterns. The square-root of the second-order cross-intensity function is shown in d, which is qualitatively very similar to Fig. 5e. Figure 6e shows the trajectory of the second-order effect for a fixed value of $u = 12$ ms (i.e. a vertical slice through the peak response in d, indicated by the arrow), where the solid curve is that obtained from 6d and the dashed is that obtained from the same value of u from 5e. The gray region surrounding the dashed curve represents the standard error, obtained by segmenting the data from Fig. 5 into thirds, which clearly demonstrates the differences in the two measures. Finally, the first-order cross-intensity estimate for this binary trial is shown in f. The range of inter-deflection intervals induces different levels of suppression through the trial, which results in cross-intensity estimates that reflect the average across the trial.

3.3. Adaptation

The stimuli described thus far have consisted of averages across repetitive deflections of vibrissa; the estimates obtained, therefore, represent steady-state behavior of the neuron in question. Importantly, many neurons in the somatosensory cortex exhibit strong adaptation to such stimuli (Ahissar et al., 2001; Chung et al., 2002). In order to determine the precise effects of this form of adaptation on the input/output relationship, we presented cells with square wave deflection patterns, interleaved with periods of rest, an example of which is summarized in Fig. 7. As described in the

methods section, the stimulus can be described mathematically as $d(t) = \bar{d}s_{\gamma_s}(f_s t)s_{\gamma_a}(f_a t)$, where for this case $\gamma_s = \gamma_a = 0.5$, and the frequencies f_s and f_a were 5 and 0.5 Hz, respectively. The ISI histogram is shown in a. This particular cell exhibited a strong response to the rising edge, and a less vigorous response to the falling edge of the stimulus. This is reflected in the peak of the ISI histogram at 200 ms (as indicated with the arrow) and little or no peak at 100 ms. Ignoring the adaptation effects, the cross-intensity function for the rising edge response can be estimated, as shown in b. To illustrate the adaptation effect, the raster plot for the “on” portion of the adapting stimulus is shown in c. The curves in d further illustrate the gross effect, where the top panel represents the relative firing rate over 50 ms following the rising edge, as a function of time during the adapting stimulus, normalized by the response in the first stimulus cycle. The bottom plot represents the latency to peak response over the adapting stimulus (note that this is different from latency to first spike). There is a clear attenuation in the response and a corresponding increase in the latency, that was observed across most cells (although in some cases, the latency shifts were not as dramatic). The estimates in e illustrate the cross-intensity estimate, $m_{XY}(t_1, t_2)$

described in Eq. (7) in the methods section. Estimates are shown for t_1 of 0, 200, 400, 600, and 800 ms, with corresponding lags of $u = t_2 - t_1$ from 0 to 100 ms (total vertical scale ranging from 0 to 7, same as in the bottom panel of b). The values of t_1 represents the absolute time of the beginning of each cycle within the periodic stimulus, whereas u represents the time relative to the beginning of each cycle. This sequence of estimates shows a clear attenuation that is most dramatic in the first two cycles and a clear shift in the response latency as reflected in the location of the peak of the cross-intensity estimate. Importantly, note that the cross-intensity estimate of b is representative of the average across the adapting stimulus, and closely resembles the estimate at 400 ms shown in e.

4. Discussion

Point process descriptions of neuronal firing are particularly relevant in regimes of sparse coding, where rate descriptions are not appropriate. This was first explored more than three decades ago in both single-unit and neuronal population studies (Gerstein and Kiang, 1960; Perkel et al., 1967a, 1967b; Marmarelis and Naka, 1973a, 1973b; Brillinger et al., 1976). Although

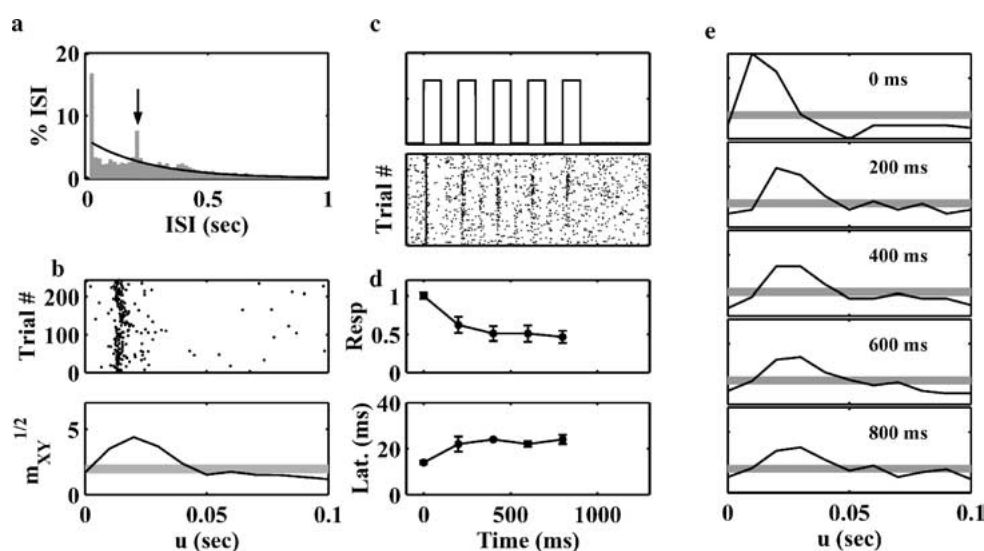


Figure 7. Adaptation. The adapting stimulus consisted of 5 cycles (1 second) of a 5 Hz square wave pattern, interleaved with 1 second of “rest”. (a) The ISI histogram (arrow indicates peak at 200 ms). (b) The raster and corresponding square-root cross-intensity function between the rising edge and neuronal response is shown ($h = 10$ ms), neglecting adaptation effects. Horizontal axis, u , is time since rising edge deflection. (c) Effects of the adaptation, where the top plot shows the stimulus ($700 \mu\text{m}$ max deflection), and the bottom plot shows the corresponding raster. (d) The mean firing rate (over 50 ms, normalized to first cycle, top) and latency to peak response (bottom) are shown as functions of the cycle number. (e) Adaptation effects on the square-root cross-intensity function at different stages of the stimulation ($h = 10$ ms; horizontal axis is time since rising edge deflection for each cycle, vertical axis range for each is 0–7). For all panels, depth = $700 \mu\text{m}$ and primary whisker E4.

these approaches have continued to flourish in population coding studies, subsequent experimental studies of sensory-evoked single-unit activity have primarily relied on rate-based descriptions of neuronal coding, perhaps due to the relative obscurity of counting process descriptions and the corresponding complexity of analyses involving combinations of continuous and discrete processes. More recent studies have begun to again revisit this topic in a number of different experimental contexts (Frank et al., 2000; Kass and Ventura, 2001; Jarvis and Mitra, 2001). Here, we have presented a non-parametric description of cortical point events, both through auto-generative processes in the absence of external input, and through the influence of exogenous sensory inputs. The intensity estimates revealed a strong second-order relationship that defines the tuning characteristics in response to patterns of tactile stimuli. One intrinsic value of the method of analysis presented here is the ability to subsequently predict/simulate neuronal spike trains directly from the characterization. Deviations from Poisson-like behavior are captured in the intensity functions that are conditioned on the previous spiking activity. As with most methods of spike-train analysis, however, this approach involves temporal bins, here denoted as h . The width of this temporal bin directly influences this analysis; vanishingly small bins, on the order of the refractory period, result in measures more indicative of the point-event structure, whereas increasingly large bins approach rate-based characterizations. We would argue, therefore, that the approach presented here makes few assumptions as to the underlying relevant encoding strategy, and that by varying the binning parameter, the continuum between rate- and temporally-based coding schemes can be explored.

Putative excitatory cortical neurons typically have extremely low spontaneous firing rates, in contrast to many “upstream” neurons (Brumberg et al., 1996). One immediate question is whether this is an intrinsic property of cortical neurons, or instead a function of the cortical network. Previous studies of the thalamocortical circuit suggest that at least some portion of the post-excitatory suppression observed in the cortex is inherited from the thalamic projections (Kyriazi and Simons, 1993; Kyriazi et al., 1994). The abundance of intracortical inhibition, however, serves to enhance cortical specificity through narrowing of tuning properties that first arise through feedforward connectivity. In addition, after-hyperpolarization effects that are related to slow intrinsic conductance changes of the cells and

activity modulated mechanisms of synaptic depression are also present (Chung et al., 2002). Most likely, the observations here reflect some combination from these sources and others. Here we have shown that the correlation structure of spontaneous activity alone reflects the same type of suppressive characteristics demonstrated in cortical responses driven by exogenous input. High-order structure observed during sensory stimulation was not revealed through spontaneous activity (data not shown), perhaps due to the limited lengths of the data set. It is also possible that the structure is not revealed through spontaneous activity because the inhibitory neurons in layer 4 require thalamic input to fire; without the synchronous activity induced through stimulus-locked thalamic input, the effect is less dramatic and thus the higher-order structure less apparent.

The effect of the prolonged suppression induced by previous activity was first shown in Fig. 4h, but presented in more detail in Fig. 5. This prolonged suppression has been previously demonstrated in both extracellular (Kyriazi et al., 1994) and intracellular (Zhu and Connors, 1999) studies, and has been shown in some cases to last as long as 1.4 seconds. The top row of Fig. 5 illustrates that the correlation structure in the spontaneous activity revealed through the auto-intensity estimates would predict such a suppression to secondary stimuli within a 50 ms time window (although this varied from cell to cell). These second-order effects can be estimated directly from neuronal responses to deflection patterns of random intervals, as illustrated in Fig. 6d and e. The second-order cross-intensity evaluated at the value of $u = 12$ ms for which the function was maximal exhibited the same qualitative trend as the same function generated from separate trials of square wave stimuli with varying duty cycle (Fig. 6e). One fundamental difference between these two situations to note is that in the trials where the duty cycle was varied, the two deflections (rising and falling edges) were not preceded directly by any other stimuli, but instead had a prolonged period of rest (≥ 900 ms), whereas the random pattern of deflections introduced even higher-order effects related to previous activity. When the first-order cross-intensity function was computed from the response to the binary pattern, without taking into account the temporal effects of the prolonged suppression, the function tended to be underestimated as compared to the presentation of the deflection in the absence of these higher order effects, as illustrated in Fig. 6f.

The above discussion focuses on representations that are stationary over time. However, adaptation is a ubiquitous characteristic of all sensory pathways; sensory pathways continuously readjust/rescale on a number of different time scales in response to changing properties in the external world. Point process models have only recently been utilized to describe adaptive neural systems, most notably in the rat hippocampus (Brown et al., 2001; Frank et al., 2002). In the rat vibrissa system, adaptation to repetitive stimuli, occurring on the time scale of seconds, has been observed in both thalamic and cortical investigation (Ahissar et al., 2001; Chung et al., 2002). Here, we found that the effect of the adaptation to the periodic stimulus is dramatic in cortical neurons, and seems to be fairly rapid in onset, reaching steady state by the second or third cycle of the stimulus, consistent with other recent studies (data shown for one cell, but observed across the population). Importantly, the cross-intensity between stimulus and response can be computed in a manner that relaxes the assumption of stationarity of response, resulting in an evolution of the temporal dynamics, as shown in Fig. 7e. The modest increase in latency, but strong attenuation of the cross-intensity function is clearly illustrated with this example. Although typically defined in the context of periodic stimuli, this phenomena is likely to be important in nearly all patterns of sensory stimulation that invoke higher-order interactions, such as the palpation of surface textures during normal behavior.

In summary, the approach we present here is based on descriptive measures for stochastic point processes. Both the neuronal activity, and the corresponding discrete “all-or-none” nature of the vibrissa deflection, are well-described in this context. The correlation structure revealed by the intensity measures introduced here reflects the interplay between excitatory and suppressive influences, which together define neuronal response characteristics to temporally structured stimuli. Post-spike suppression can be directly determined from spontaneous neuronal activity, and can be used to predict second-order effects observed when the vibrissa are deflected in rapid succession. Although these effects are likely to arise from a combination of a number of different biophysical mechanisms that may not be possible to decouple, the importance of the resulting functional characterization lies in the potential for predicting a number of experimentally observed phenomena and suggesting further hypotheses that can be tested experimentally.

Acknowledgments

RMW was supported by a National Science Foundation Pre-doctoral fellowship. We thank Alireza Seyed Bolori and two anonymous reviewers for helpful comments in the preparation of this manuscript.

References

- Ahissar E, Sosnik R, Bagdasarian K, Haidarliu S (2001) Temporal frequency of whisker movement. ii. Laminar organization of cortical representations. *J. Neurophysiol.* 86: 354–367.
- Brillinger DR, Bryant HL, Segundo JP (1976) Identification of synaptic interactions. *Biol. Cybernetics* 22: 213–228.
- Brown EN, Nguyen DP, Frank LM, Wilson MA, Solo V (2001) An analysis of neural receptive field plasticity by point process adaptive filtering. *PNAS* 98: 12261–12266.
- Brumberg JC, Pinto DJ, Simons DJ (1996) Spatial gradients and inhibitory summation in the rat whisker barrel system. *J. Neurophysiol.* 76: 130–140.
- Brumberg JC, Pinto DJ, Simons DJ (1999) Cortical columnar processing in the rat whisker-to-barrel system. *J. Neurophysiol.* 82: 1808–1817.
- Carvell GE, Simons DJ (1990) Biometric analysis of vibrissal tactile discrimination in the rat. *J. Neurosci.* 10: 2638–2648.
- Carvell GE, Simons DJ (1996) Abnormal tactile experience early in life disrupts active touch. *J. Neurosci.* 15: 2750–2757.
- Chung S, Li X, Nelson SB (2002) Short-term depression at thalamocortical synapses contributes to rapid adaptation of cortical sensory responses in vivo. *Neuron* 34: 1–20.
- Cox DR, Isham V (1980) *Point Processes*. Chapman and Hall, London.
- Frank LM, Brown EN, Wilson MA (2000) Trajectory encoding in the hippocampus and entorhinal cortex. *Neuron* 27: 169–178.
- Frank LM, Eden UT, Solo V, Wilson MA, Brown EN (2002) Contrasting patterns of receptive field plasticity in the hippocampus and the entorhinal cortex: An adaptive filtering approach. *J. Neurosci.* 22(9): 3817–3830.
- Gerstein GL, Kiang NY-S (1960) An approach to the quantitative analysis of electrophysiological data from single neurons. *Biophys. J.* 1: 15–28.
- Ghazanfar AA, Stambaugh CR, Nicolelis MAL (2000) Encoding of tactile stimulus location by somatosensory thalamocortical ensembles. *J. Neurosci.* 20: 3761–3775.
- Guic-Robles E, Valdivieso C, Guajardo G (1989) Rats can learn a roughness discrimination using only their vibrissal system. *Behavioural Brain Research* 31: 285–289.
- Ito M (1981) Some quantitative aspects of vibrissa-driven neuronal responses in rat neocortex. *J. Neurophysiol.* 46(4): 705–715.
- Jarvis JR, Mitra PP (2001) Sampling properties of the spectrum and coherency of sequences of action potentials. *Neural Computation* 13: 717–749.
- Kass RE, Ventura V (2001) A spike-train probability model. *Neural Computation* 13: 1713–1720.
- Kyriazi HT, Carvell GE, Simons DJ (1994) Off response transformations in the whisker/barrel system. *J. Neurophysiol.* 72: 392–401.
- Kyriazi HT, Simons DJ (1993) Thalamocortical response transformations in simulated whisker barrels. *J. Neurosci.* 13: 1601–1615.

- Lewicki MS (1998) A review of methods for spike sorting: The detection and classification of neural action potentials. *Network: Computation in Neural Systems* 9: R53–R78.
- Lichtenstein SH, Carvell GE, Simons DJ (1990) Responses of rat trigeminal ganglion neurons to movements of vibrissae in different directions. *Somatosensory and Motor Research* 7(1): 47–65.
- Marmarelis P, Naka KI (1973a) Non-linear analysis and synthesis of receptive field responses in the catfish retina. i. Horizontal cell-ganglion chains. *J. Neurophysiol.* 36: 605–618.
- Marmarelis P, Naka KI (1973b). Non-linear analysis and synthesis of receptive field responses in the catfish retina. ii. One-input white-noise analysis. *J. Neurophysiol.* 36: 619–633.
- Moore C, Nelson S (1998) Spatio-temporal subthreshold receptive fields in the vibrissa representation of rat primary somatosensory cortex. *J. Neurophysiol.* 80(6): 2882–2892.
- Nicolelis M, Chapin J (1994) Spatiotemporal structure of somatosensory responses of many-neuron ensembles in the rat ventral posterior medial nucleus of the thalamus. *J. Neurosci.* 14: 3511–3532.
- Perkel D, Gerstein G, Moore G (1967a) Neuronal spike trains and stochastic point processes. i. The single spike train. *Biophysical Journal* 7(4): 391–418.
- Perkel DH, Gerstein GL, Moore GP (1967b) Neuronal spike trains and stochastic point processes. ii. Simultaneous spike trains. *Biophysical Journal* 7(4): 419–440.
- Pinto DJ, Brumberg JC, Simons DJ (2000) Circuit dynamics and coding strategies in rodent somatosensory cortex. *J. Neurophysiol.* 83: 1158–1166.
- Simons DJ (1978) Response properties of vibrissa units in rat S1 somatosensory neocortex. *J. Neurophysiol.* 41: 798–820.
- Simons DJ (1983) Multi-whisker stimulation and its effects on vibrissa units in rat S1 barrel cortex. *Brain Research* 276: 178–182.
- Simons DJ, Carvell GE (1989) Thalamocortical response transformation in the rat vibrissa/barrel system. *J. Neurophysiol.* 61(2): 311–330.
- Welker C (1971) Microelectrode delineation of fine grain somatotopic organization of (S1) cerebral neocortex in albino rat. *Brain Res.* 26(2): 259–275.
- Zhu JJ, Connors BW (1999) Intrinsic firing patterns and whisker-evoked synaptic response of neurons in the rat barrel cortex. *J. Neurophysiol.* 81: 1171–1183.